Applied Thermal Engineering 213 (2022) 118804

Contents lists available at ScienceDirect

Applied Thermal Engineering

journal homepage: www.elsevier.com/locate/apthermeng

Visualization study on the uniformity of refrigerant distribution in parallel multi-channels

Yuqi Huang [a,b], Caifeng Wei [a], Shun Wang [a], Yiji Lu [c,*]

[a] Department of Energy Engineering, Zhejiang University, Hangzhou 310027, Zhejiang, China
[b] State Key Laboratory of Clean Energy Utilization, Department of Energy Engineering, Zhejiang University, Hangzhou 310027, China
[c] James Watt School of Engineering, University of Glasgow, Glasgow G12 8QQ, United Kingdom

ARTICLE INFO

Keywords:
Heat pump thermal management
Two-phase flow
Maldistribution
Image processing
Flow pattern

ABSTRACT

Heat pump technology is a battery thermal management technology with considerable potential and which has obvious advantages in environmental adaptability and energy saving. The small-channel heat exchanger is an important part of the heat pump system, and the uniformity of the two-phase refrigerant in the header and branch channels is one of the key issues that restrict the performance of the system. In this paper, a two-phase flow visualization phase separation experimental platform, with R1233zd(E) as the working fluid, was established to study the refrigerant distribution in small parallel multi-channels (3 mm). Three inlet configurations are designed, and two types of operating conditions are tested. Moreover, the gas-liquid two-phase boundary in channels is extracted to calculate the average void fraction based on the OpenCV graphics processing function libraries. The key conclusions of the current study are as follows: (1) The two-phase distribution uniformity under the lower inlet method is improved by 50–90% compared with the middle inlet and upper inlet methods. (2) A superior gas-liquid two-phase distribution in channels can be achieved under lower inlet quality (0.01) and lower inlet mass flux (300 kg/(m^2•s)). (3) The average void fraction in each channel is almost always positively correlated with the average pressure gradient.

1. Introduction

New energy vehicles, especially pure Electric Vehicles (EV), are envisaged to be a long term development trend. A Battery Thermal Management System (BTMS) is essential to maintain the battery temperature and the temperature difference among the modules in an appropriate range in order to achieve an improved performance [1]. The current demand for high-rate charging and discharging application scenarios of high-energy-density power batteries (such as fast charging, high-power climbing) is a challenge for BTMS. According to the different heat transfer mediums, battery thermal management technology can be mainly divided into four categories: air cooling, liquid cooling, phase change material cooling and direct cooling heat pump technology [2]. Compared with other battery cooling systems [3–5], the direct cooling heat pump technology has obvious advantages in terms of environmental adaptability, vehicle weight, cooling capacity and safety [6]. Given the current arrangement of most battery modules in the vehicle, the small-channel heat exchanger for heat pump thermal management is usually adopted, which involves multiple branches connected in parallel to the header, so that the heat transfer coefficient can be maintained at a high level whilst the pressure drop on the refrigerant side will not be too great [7,8]. However, this kind of arrangement usually results in the problem of uneven two-phase distribution in channels, which will degrade the performance of the heat exchanger to a large extent [9]. For example, it has been found that the maldistribution of two-phase refrigerant R410A in a parallel heat exchanger could result in 61% thermal degradation [10]. Therefore, it is crucial to determine the mechanism of maldistribution of the two-phase refrigerant inside the cold plate type heat exchanger, which will be helpful when determining the optimal design of the configuration and the operating condition of the cold plate type parallel flow two-phase heat exchanger.

To date, a number of research studies [11–13] have tried to establish simulation models to restore and predict experimental results. However, due to the complex internal mechanisms that affect the flow distribution and phase separation of multiphase flow, there seems to be no simple and reliable simulation method to accurately simulate the phase separation behavior of the two-phase refrigerant in the header. Indeed, most of the studies working on this question are performed by experimentation. In recent years, scholars have mainly focused on three main

* Corresponding author.
E-mail address: yiji.lu@glasgow.ac.uk (Y. Lu).

https://doi.org/10.1016/j.applthermaleng.2022.118804
Received 14 December 2021; Received in revised form 8 May 2022; Accepted 6 June 2022
Available online 9 June 2022

Nomenclature

Abbreviations

BTMS	Battery Thermal Management System
EV	Electric Vehicles
GWP	Global Warming Potential
HVAC	Heating Ventilation Air Conditioning
ODP	Ozone Depression Potential
ROI	Region of Interest
RSD	Relative Standard Deviation

Subscripts

c	channel
i	the i-th branch
in	inlet
l	liquid
p	pixel
s	saturation
sh	superheated
su	superficial
sub	subcooled
v	vapor, velocity

Greek letters

α	void fraction
β	the ratio of the gas phase area to the channel area in the shooting section
γ	the ratio of the average length of the gas slug to the length of the channel in the shooting section
ρ	density, kg/m^3

Symbols

A	area, m^2
d	hydraulic diameter, m
G	mass flux, kg/(m^2•s)
h	enthalpy, J/kg
l	slug or bubble length, m
L	channel length, m
$\dot{m}$	mass flow rate, kg/s
P_{w1}	power of the preheater, W
P_{w2}	power of the heater, W
P	pressure, Pa
ΔP	pressure jump, Pa
r	slug or bubble radius, m
R	channel radius, m
x	quality

aspects: the configuration methods, the geometric parameters and the operating conditions of the two-phase parallel flow heat exchangers. Many studies have been conducted on the influence of the configuration methods, including the orientation of heat exchangers, the inlet method of heat exchangers and the configuration of internal spoilers on the uniformity of the two-phase refrigerant distribution. Kim et al. [14] utilized a brazed aluminum parallel flow heat exchanger, using R134a as the working fluid, to explore the influence of the three different inlet and outlet methods (parallel, normal and vertical) on the uniformity of the two-phase refrigerant distribution, and found that under the experimental conditions, the vertical inlet method was conducive to the distribution of both the gas and liquid two-phase flow, while the parallel inlet method was only conducive to the distribution of the liquid phase, and the normal inlet method was only conducive to the distribution of the gas phase. Madanan et al. [15], using water and air as working fluid in similar heat exchangers, designed three kinds of inlet and outlet type, and found that the two-phase flow separation behavior is heavily dependent on the inlet and outlet configuration and inlet flow regimes. Kim et al. [16] designed a horizontally arranged cold plate heat exchanger for EV battery heat pump system, and studied the influence of different inlet orientations and inclination of the cold plate on the uniformity of two-phase R134a distribution. The results showed that the inclination of the heat exchanger has a greater impact on the flow distribution than the inlet orientation, but these effects are weakened as the inlet mass flow rate increases. By inserting a special perforated flute-shaped spoiler in the header, Marchitto et al. [17] explored the influence of the angle and the position of outlet holes on the flow rate and pressure drop distribution of water and air two-phase flow in the branches. The research results showed that the most uniform water and air distribution can be achieved when the spoiler outlet and the branch pipe inlet are in opposite directions. Kim et al. [10] found that the thermal degradation of the heat exchanger could be reduced from 61% to 14% by inserting a concentric perforated tube in the header using R134a. Wu et al. [18] determined that using a spoiler tube with symmetrical aperture (large diameter holes in the middle and gradually smaller diameter holes at both ends) has the best gas-liquid two-phase uniformity in the branches.

As for geometric parameters, studies concentrated on the influence of the diameter and the shape of the branch and the header, the branch spacing and quantity, and the depth of the branch inserted into the header. Zhang et al. [19] analyzed the effects of different inclined angles and channel numbers on the performance of the cold plate, and found that the inclined channel cold plate with odd channel numbers achieved better performance in BTMS. Research by Liu et al. [20] showed that the phase distribution in each branch depends largely on the branch spacing, and the inlet conditions have a greater impact on the uniformity of the phase distribution when there is a small branch spacing. Marchitto et al. [21] indicated that when the branch is inserted into the header at an appropriate depth, the uniformity of the gas-liquid two-phase distribution in the heat exchanger can be greatly improved. Operating conditions also have a significant influence on the flow distribution in each branch. Li et al. [22] investigated the influences of the hole diameter, header height and inlet mass flow rate on the liquid-separation efficiency using the multi-factor analysis [23,24] and obtained a correlation of liquid-separation efficiency based on the simulation data from the orthogonal experiments. Zou et al. [25,26] performed experiments with different inlet mass flux and inlet quality data using R134a and R410A, respectively. The results of the two mediums were comparable, and when the inlet mass flow rate is high in conjunction with a low inlet quality, a more uniform two-phase distribution occurred. This occurs because the liquid phase refrigerant with higher momentum can more easily reach the highest outlet branch in that operating condition. Redo et al. [27] conducted experiments with horizontally oriented micro-channel flat tube heat exchanger and different operating conditions using R410A, and the conclusions are similar to those of Zou et al. [25,26].

It can be seen from the above research that there are many complex factors that affect the distribution uniformity of small channel two-phase heat exchangers. However, there are still many opportunities to improve and build upon the existing research. Firstly, many scholars use simple mixtures such as water and air to replace the refrigerant when exploring the phase distribution characteristics of two-phase flow in each branch of a heat exchanger. However, studies have shown that the phase separation phenomena are very different due to substantial differences in physical properties between water-air and two-phase refrigerant [28]. Secondly, the current research with a refrigerant as a working fluid has low inlet mass flux, which means it is difficult to meet the heat dissipation requirements of the current power battery under

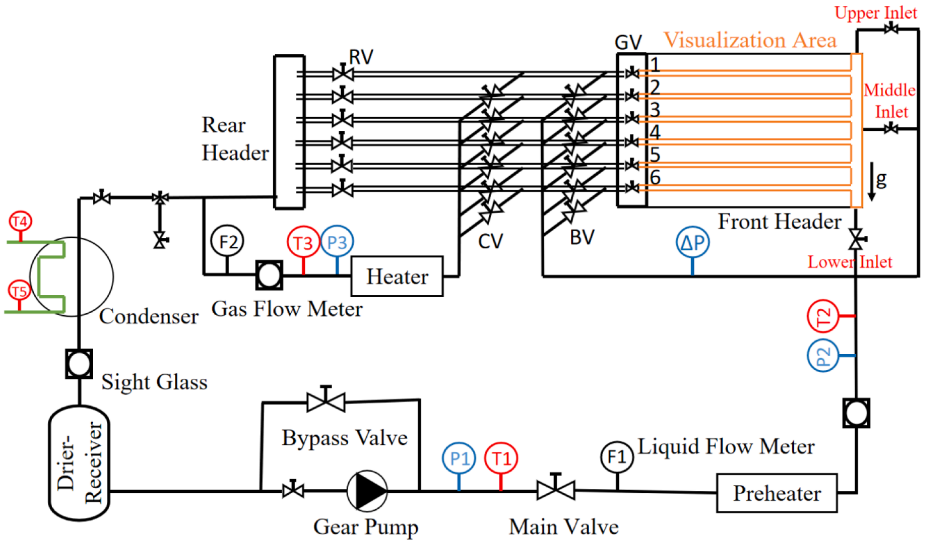

(a) Schematic drawing of the experimental platform

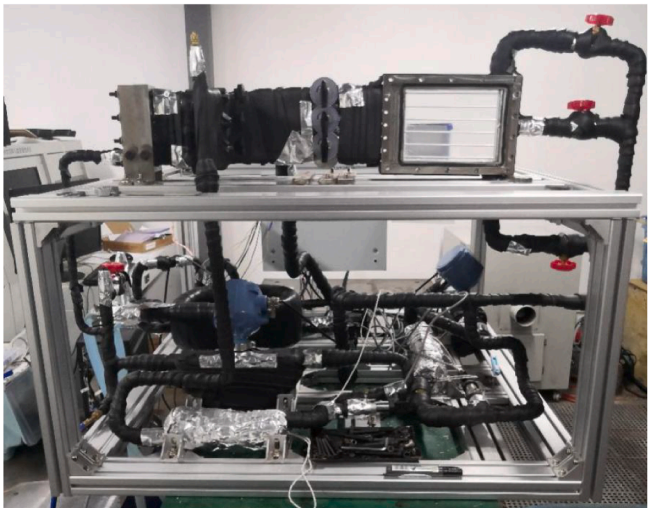

(b) Physical map of the platform

Fig. 1. Schematic diagram of the experimental platform.

Table 1
Accuracies and ranges of instrumentation devices.

Instrument	Accuracy	Range
Liquid Coriolis flowmeter	±0.2%	0.03–1366 kg/h
Vapor Coriolis flowmeter	±0.5%	0.03–1366 kg/h
Pressure transmitter	±0.5%	−0.1–1.6 MPa
Differential pressure transmitter	±0.5%	0–10 kPa
Platinum resistance thermometer sensor	±0.1 °C	0–100 °C
Power meter	±0.5%	0–7.5 KW

Table 2
Operating range and mode of experimental inlet condition parameters.

Inlet mass flux G (kg/(m^2•s))	Inlet quality x_{in} (–)	Inlet positions
300, 400, 500	0.01, 0.025, 0.04, 0.055, 0.07	Lower, Middle, Upper

high-power climbing and fast charging conditions. Finally, the method of visualization on phase separation behavior in the header and branches is helpful when observing the difference of flow pattern and phase distribution in each branch directly. In turn, this benefits the explanation of the phase separation behavior under different working conditions on the mechanism level. However, although some scholars have tried to carry out visualization research, either only the header visualization research was undertaken [27,29], or the photography lacks clarity [30]. However, new methods have been developed to assess and reconstruct the two-phase flow structure. Image analysis methods to describe the flow structure of two-phase fluid have previously been proposed. Masiukiewicz and Anweiler [31] conducted experimental measurements on a vertical rectangular channel using air-water as working medium and obtained ranges of values of the two-phase flow parameters as a function of time by dynamic image analysis method which was equipped with stereologic and videogrammetric technique. Rafałko et al. [32] studied the two-phase flow (water-glycerol and air) inside a circular minichannel using high speed recording and images correlation analysis. The results indicated that the new coefficient characterising the gas distribution changes in the minichannel was

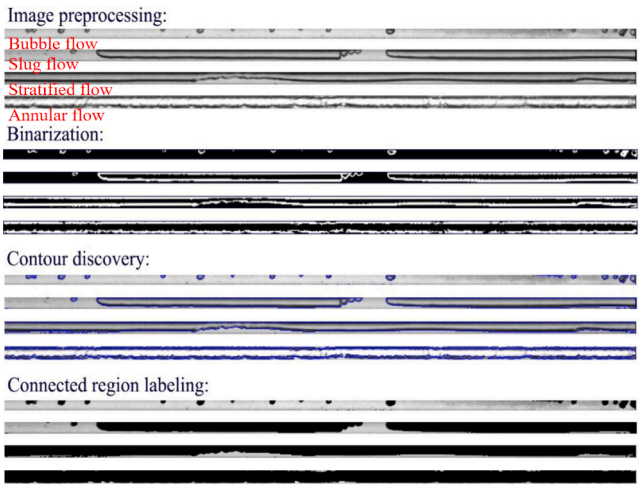

(a) Digital image processing procedures under four typical flow patterns

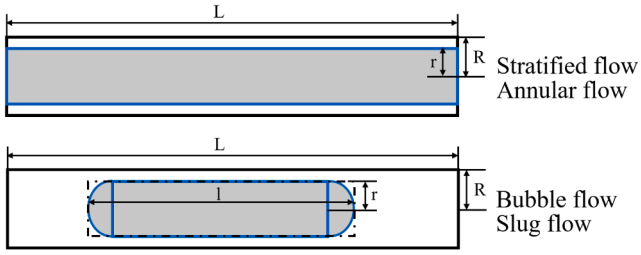

(b) Simplified schematic diagram of gas phase geometric parameters

Fig. 2. Image processing and simplified schematic diagram of four flow patterns.

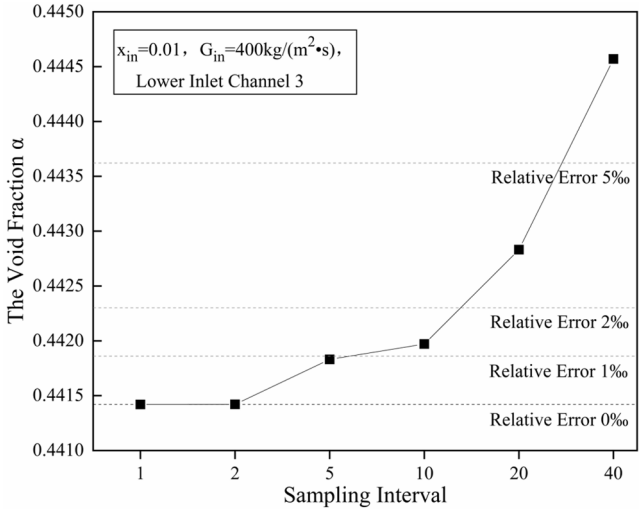

Fig. 3. The Influence of Sampling Interval on the Calculation Error of the void fraction.

applicable for a flow pattern map reconstruction. Within the scope of the authors' knowledge, no visualization research recording the phase distribution process of the two-phase refrigerant clearly and completely in a cold plate type heat exchanger for heat pump system has been conducted to date.

Therefore, in reference to a typical heat exchanger configuration of heat pump technology for the battery module [33], this research aims to identify the visualization characteristics and the associated mechanisms of flow pattern and phase distribution of a two-phase refrigerant under

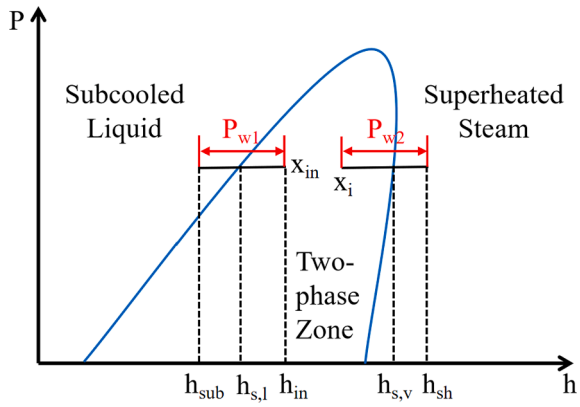

Fig. 4. Pressure-enthalpy diagram of the refrigerant in the circulation process[27].

Table 3
Visualization cases and inlet detail parameters.

Case name	Inlet method	Superficial gas velocity ($v_{v,su}$, m/s)	Superficial liquid velocity ($v_{l,su}$, m/s)	Inlet quality (x_{in})	Inlet mass flux (G_{in}, kg/(m²•s))
Case_1	Upper	0.3531	0.2375	0.01	300
Case_2	Middle	0.3531	0.2375	0.01	300
Case_3	Lower	0.3531	0.2375	0.01	300
Case_4	Lower	0.4709	0.3166	0.01	400
Case_5	Lower	1.883	0.3071	0.04	400
Case_6	Lower	3.296	0.2975	0.07	400
Case_7	Lower	0.5886	0.3958	0.01	500

Table 4
Two-phase physical parameters of the refrigerant (30 °C, 0.154 MPa).

Status	Density (kg/m³)	Viscosity (Pa•s)	Surface tension (N/m)
liquid (l)	1250.6	4.394×10^{-4}	0.0139
vapor (v)	8.495	1.124×10^{-5}	

reasonably high inlet mass flux conditions (300–500 kg/(m²•s)) with a small-channel cold plate type heat exchanger. In this work, the novelty of this study mainly covers two points, one is the visual design of all the main experimental sections, including the header and each branch channel. As the entire visual analysis of the phase separation flow in the header and branch channels has not previously been undertaken, this is an innovative aspect of this study. The second is to propose an appropriate simplified processing method, by extracting the key parameters of the gas phase flow in small channels, which is also novel. The imaging processing method is adopted to analyse the distribution of the two-phase refrigerant R1233zd(E) in each branch quantitatively. Three kinds of inlet methods (upper inlet, middle inlet and lower inlet) are set with inlet quality ranging 0.01–0.07, and with six parallel circular branch channels constantly connected to a circular header. The inlet quality is defined as the ratio of the inlet mass flow rate of gaseous working medium to the inlet total mass flow rate of working medium per unit time. The results and conclusions of this study can provide reference information for the optimization design of two-phase flow heat exchangers for the battery heat pump system of new energy vehicles.

2. Experimental method and data reduction

2.1. Experimental platform and facility

Fig. 1 shows the schematic diagram of the experimental platform. As

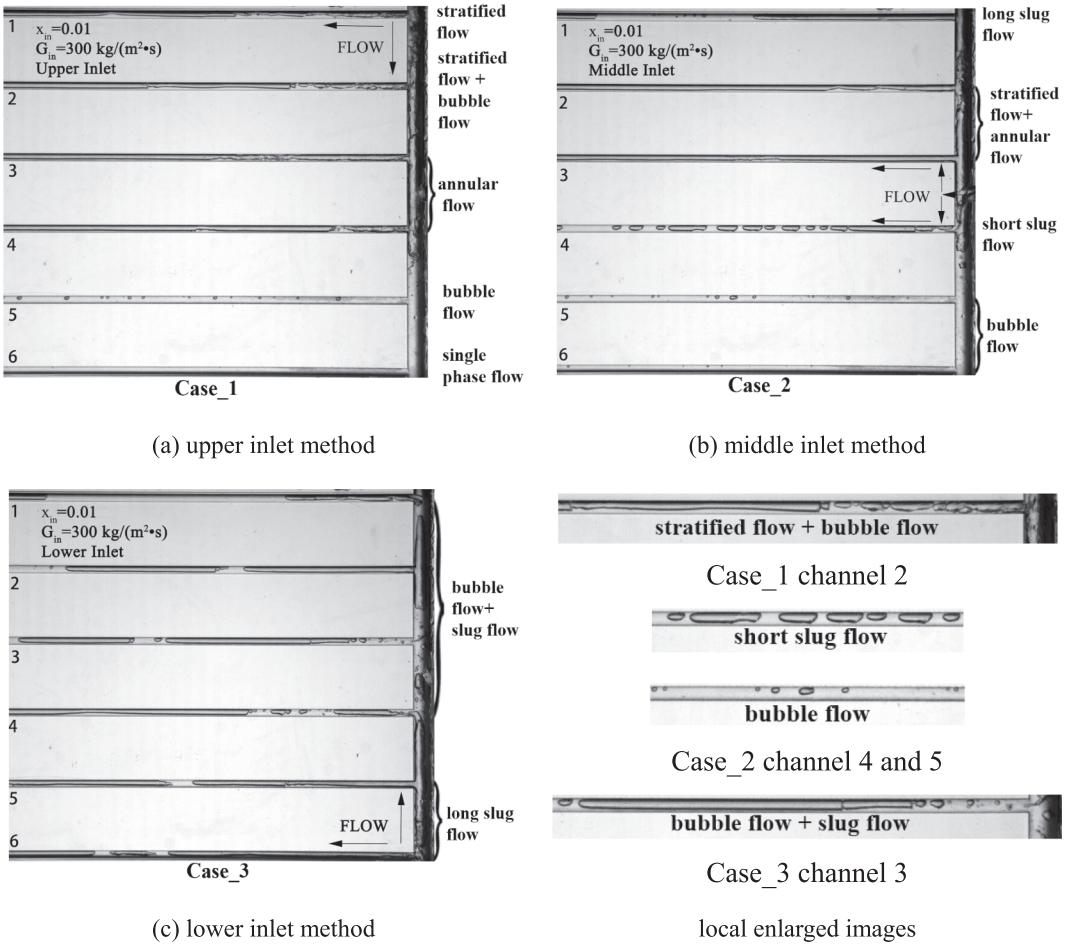

Fig. 5. Typical phase distribution and local enlarged images under different inlet methods.

shown in Fig. 1(a), the whole experimental loop can be divided into a driving section, measuring section and visual phase separation section. The header and branch channels of the test sections are arranged vertically in this study [34–36]. The subcooled refrigerant enters the liquid Coriolis flowmeter under the drive of the magnetic gear pump. Before passing through the one of three inlet valves of the visualization zone, the refrigerant is heated by the pre-heater to reach a certain quality. Then the two-phase refrigerant enters the inlet header, separated by vertically arranged six-channel branch pipes. Next, the refrigerant is collected by the rear header and cooled by the water in an external chiller circuit to subcooled state. Finally, the refrigerant returns to the magnetic drive gear pump, thus completing a cycle.

The experiment platform has two measurement branches. The first branch is led out through the bypass valve BV, and the pressure drop ΔP_i ($i = 1, 2–6$) between the inlet and each branch can be measured by a differential pressure sensor on the branch. The second branch is led out through the bypass valve CV, where a heater and a gas Coriolis flow meter are installed to heat the refrigerant to superheated state and measure the total mass flow rate of each branch accurately. The heating power of the heater is adjusted by the voltage via a voltage regulator connected at both ends of the heating rod, and is measured by a power meter. The accuracies and ranges of the measuring instruments used in this experiment are shown in Table 1.

In order to better observe the phase and mass flow separation process, the cold plate type heat exchanger consists of transparent acrylonitrile butadiene styrene copolymers and produced 3D printing. The overall size of the heat exchanger is 195*140*10 mm^3, and there are three circular inlet positions, which are located in the lower right corner (lower inlet), middle right (middle inlet) and upper right corner (upper inlet). The diameter of the inlet header is 6 mm, and the distance between the six branches is 25 mm. Considering the pressure drop and heat transfer performance of the refrigerant in channels, the diameter of the six circular branches is set to 3 mm [16]. A high-speed camera (Photron Fastcam AX100, Japan) is used to capture the phase separation process. The shooting section is the visualization area including the header and each branch channel.

2.2. Experiment object and measurement procedures

Currently, the most widely used refrigerant in the vehicle Heating Ventilation Air Conditioning (HVAC) system is R134a, but it has been included in the Kigali Amendment list [37], and so is likely to be gradually eliminated in the future. Therefore, it is important to urgently develop a new type of refrigerant suitable for EV HVAC systems and heat pump thermal management systems. The experiment object of this paper is the fourth-generation environmentally friendly refrigerant R1233zd(E), which has relatively high latent heat of evaporation and critical temperature (165.6 °C).

The overall test conditions of this experiment are shown in Table 2. When an experimental condition is running in a stable condition, the bypass valves CV and BV are closed while the branch valves RV and the scaled disc fine-tuning valve GV are all open at first. To measure the mass flow of the i-th branch, the bypass valve BV_i should be turned on first, then the bypass valve CV_i should be turned on and finally, the branch valve RV_i should be turned off. The power of the heater P_{w2} should be adjusted to an appropriate value to ensure that the refrigerant in this branch is overheated. Then the scaled disc valve GV_i should be fine-tuned to maintain the pressure jump ΔP_i at the same level. When

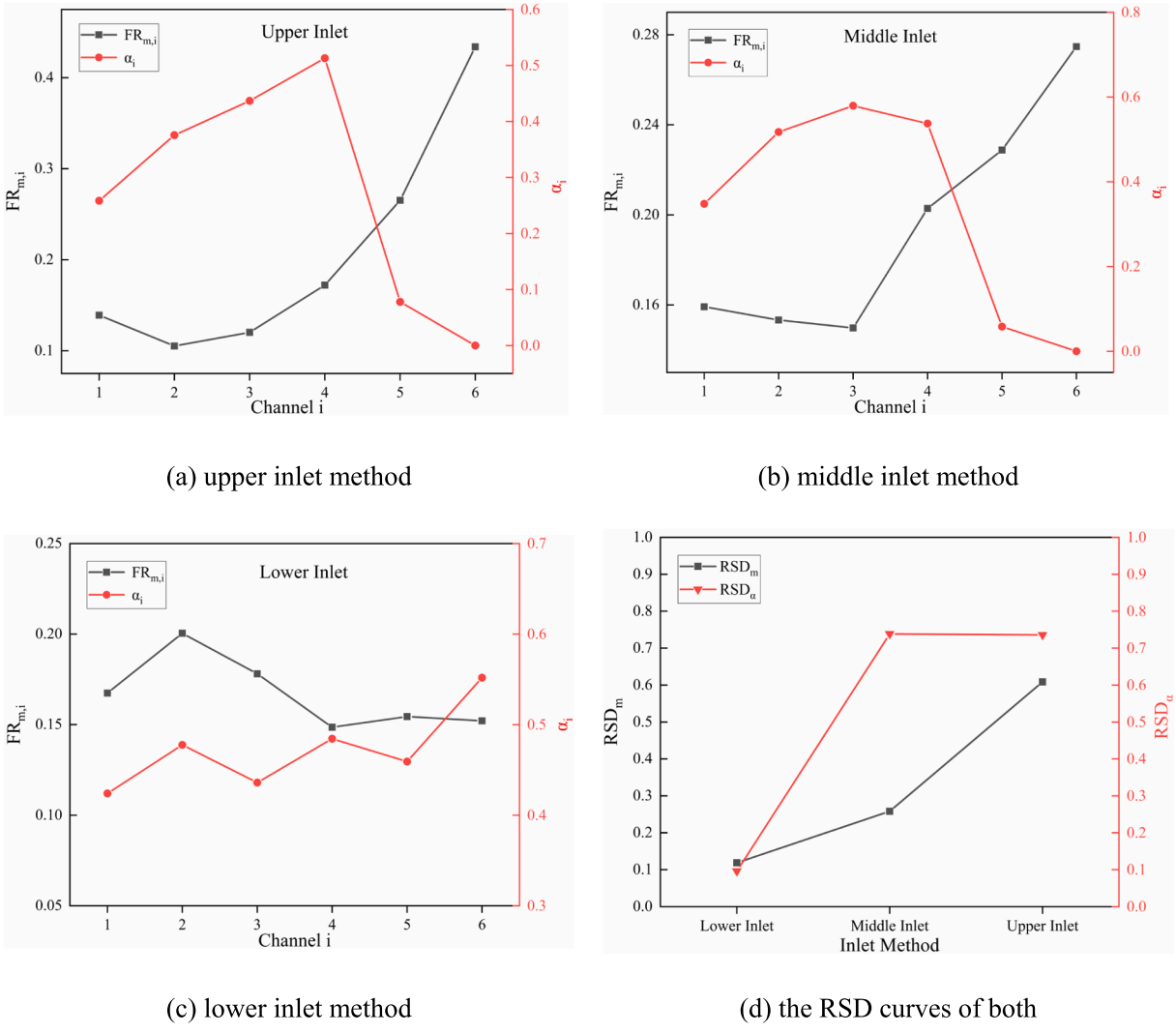

Fig. 6. The quantitative distribution and RSD curves under different inlet methods.

the pressure drop of the channel to be measured is kept steady, it can be considered that the impact of the measurement branch can be ignored [27].

2.3. Digital image processing procedures and data reduction

The captured flow image of the two-phase working fluid in small channels in this study has a relatively clear gas-liquid interface, so a series of image processing methods can be used to capture the gas phase in a two-phase flow. Using the rich library functions provided by OpenCV for processing digital images, batch processing of captured digital images can be performed efficiently. For the four typical two-phase flow patterns that appeared in this study, image processing procedures including image preprocessing, binarization, contour discovery and connected region labeling are shown in Fig. 2(a).

At the image preprocessing stage, image cropping and rotation are adopted to determine the ROI (Region of Interest). Then the Otsu threshold algorithm is adopted to further enhance the image by simply binarizing the obtained grey image. Finally, some relative algorithms provided by OpenCV can be adopted to discover the contours and label the connected regions. For each gas phase connected region, the pixel area can be calculated, and the length of the gas slug can be estimated by calculating the length of the circumscribed rectangle, which provides key characteristic data for the calculation of the average void fraction.

The void fraction α is defined as the proportion of the area occupied by the gas on the flow direction, that is:

$$\alpha = \frac{A_v}{\frac{\pi}{4}d^2} \tag{1}$$

The void fraction α, which is the key factor for predicting the two-phase pressure drop, density, viscosity, actual velocity, and heat transfer coefficient, is an important parameter describing two-phase flow [38]. According to relevant literature, void fraction α and gas volume fraction (defined as the ratio of gas volume flow to total volume flow) are positively correlated. Therefore, the void fraction α can be used to characterize the relative amount of gas in the channel. Combining the actual flow conditions within the scope of this study, a suitable simplified treatment method for calculating the void fraction α is proposed as follows:

As shown in Fig. 2(b), for stratified flow and annular flow, the gas phase occupies the entire channel in the length direction. In order to simplify the calculation, the gas phase is averaged into a rectangle according to the pixel area it occupies (shown by the gray shaded area). Through the image processing method of the gas phase area, the pixel occupied area $A_{p,v}$ and $A_{p,c}$ of the gas phase area and the entire channel area can be obtained respectively. And they can be calculated as:

$$A_{p,v} = 2rL \tag{2}$$

$$A_{p,c} = 2RL \tag{3}$$

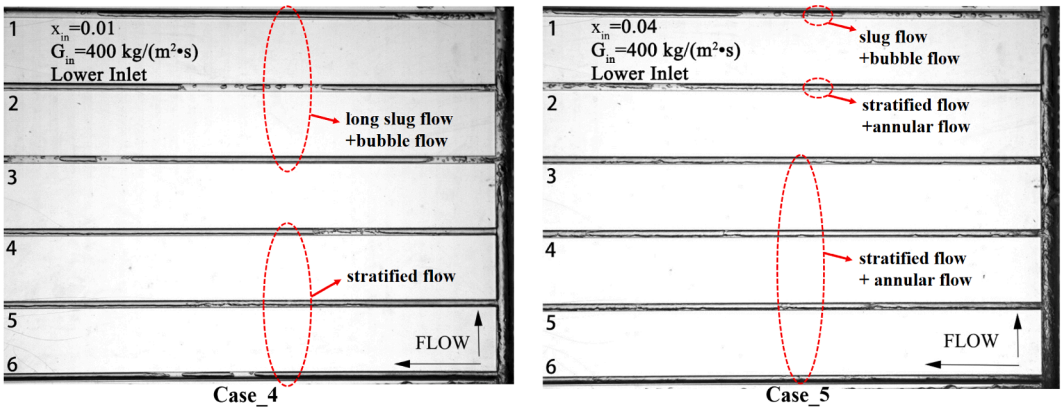

(a) x_{in}=0.01 (b) x_{in}=0.04

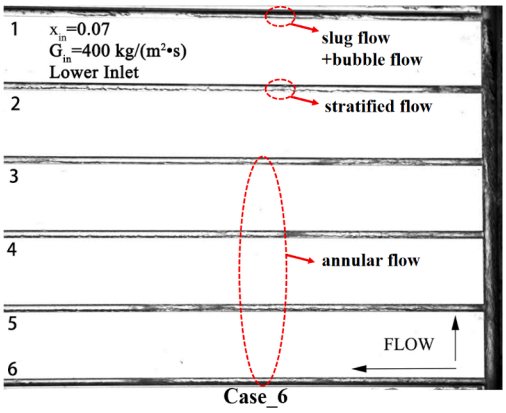

(c) x_{in}=0.07

Fig. 7. Typical phase distribution images under different inlet quality data.

Define the ratio of the gas phase area to the channel area in the shooting section under the flow pattern, as the coefficient β_1:

$$\beta_1 = \frac{A_{p,g}}{A_{p,c}} = \frac{r}{R} \tag{4}$$

In the actual three-dimensional flow process in a circular tube, the gas phase area is equivalent to a cylinder with a bottom radius of r and a height of L. According to the definition of the void fraction, the calculation formula for the average void fraction α_1 in this case is obtained as:

$$\alpha_1 = \frac{\pi r^2 L}{\pi R^2 L} = \beta_1{}^2 \tag{5}$$

And as for bubble flow and slug flow shown in Fig. 2(b), the gas phase does not fill the entire channel in the length direction. Similarly, in order to simplify the calculation, the gas area is simplified as the gray shaded part (two semicircles at both ends and a rectangle in the middle). Most of the gas slugs observed in this study are long gas slugs, and the channel size is small, so this processing method will not create a significant error. Then, the calculation formula for the ratio β_2 of the gas phase area to the channel area in the shooting section is:

$$\beta_2 = \frac{A_{p,g}}{A_{p,c}} = \frac{rl}{RL} \tag{6}$$

The ratio of the average length of the gas slug to the length of the channel in the shooting section as γ is defined as:

$$\gamma = \frac{l}{L} \tag{7}$$

Similarly, in this case, the formula for calculating the average void fraction α_2 is

$$\alpha_2 = \frac{\pi r^2 l}{\pi R^2 L} = \frac{\beta_2^2}{\gamma} \tag{8}$$

Comparing Eq. (5) and (8), it can be observed that when the flow pattern is stratified or annular flow, the ratio of the length of the gas phase region to the length of the channel is 1 (i.e. $\gamma = 1$). Therefore, a unified formula can be used to calculate the average void fraction α:

$$\alpha = \frac{\beta^2}{\gamma} \tag{9}$$

Since the flow in each channel is constantly changing, the calculation of each parameter of the gas phase requires sufficient images at different times to obtain the average value of the parameters. For this study, at least 100 frames of different images are taken at each working condition to calculate the average values. Fig. 3 is the sampling interval on the analysis of the relative error of the void fraction ($x_{in} = 0.01$, $G_{in} = 400$ kg/(m^2•s), the third channel of the lower inlet). The sampling interval is defined as the difference in frame number between adjacent frames selected in a continuous video frame. It can be seen that when the sampling interval is 10 or less, the relative error of the calculation result of the void fraction α is within 2‰. With a further increase of the sampling interval, the relative error increases rapidly. In order to speed up the progress of experimental data processing and save computing resources, whilst also ensuring calculation accuracy, it is considered reasonable to set the sampling interval to 10 in this study.

In addition, for a heat exchanger with multiple outlet channels, the mass flow ratio $FR_{m,i}$ of the i-th channel is defined as:

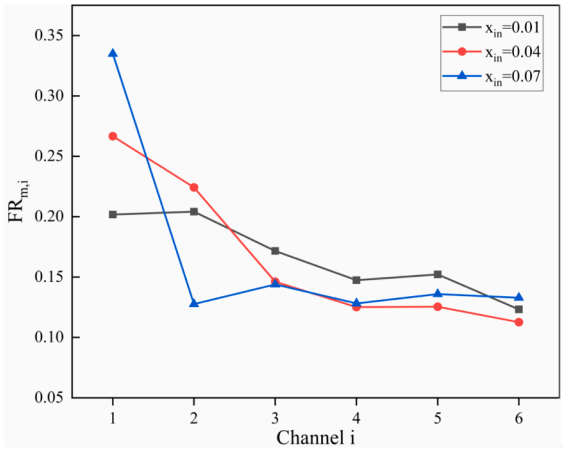

(a) the mass flow ratio distribution curves

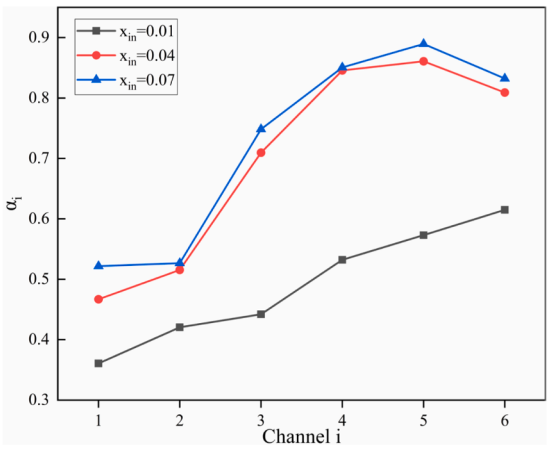

(b) the void fraction distribution curves

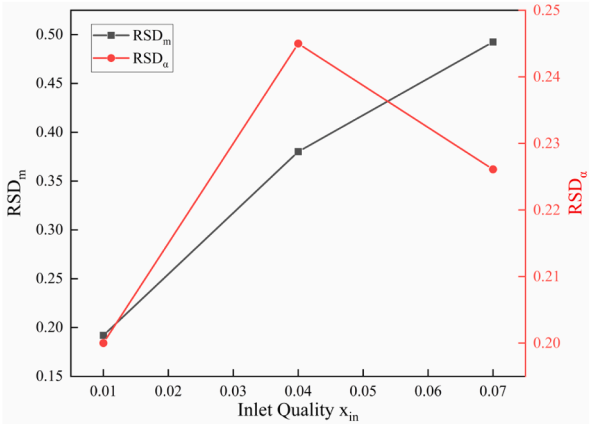

(c) the RSD curves of both

Fig. 8. The quantitative distribution and RSD curves under different inlet quality data.

$$FR_{m,i} = \frac{\dot{m}_i}{\sum_0^n \dot{m}_i} \tag{10}$$

Relative Standard Deviation (RSD) is introduced to evaluate the uniformity of the two-phase flow [25]. For mass flow ratio $FR_{m,i}$, it is defined as:

$$RSD_m = \frac{SD}{\overline{FR}_{m,i}} = \frac{\sqrt{\frac{1}{n}\sum_1^n \left(FR_{m,i} - \overline{FR}_{m,i}\right)^2}}{\overline{FR}_{m,i}} \tag{11}$$

And for average void fraction α, is defined as:

$$RSD_\alpha = \frac{SD}{\overline{\alpha}_i} = \frac{\sqrt{\frac{1}{n}\sum_1^n (\alpha_i - \overline{\alpha}_i)^2}}{\overline{\alpha}_i} \tag{12}$$

The evaluation of the quality of the inlet and outlet depends on the pressure-enthalpy diagram shown in Fig. 4. When the experimental cycle reaches a steady state, there is a limited pressure difference between the three Pressure Transmitters. Therefore, the inlet quality x_{in} can be expressed as:

$$x_{in} = \frac{h_{in} - h_{s,l}}{h_{s,v} - h_{s,l}} \tag{13}$$

The inlet enthalpy h_{in} is unknown, and can be calculated as:

$$h_{in} = \frac{P_{w1}}{\dot{m}_{in}} + h_{sub} \tag{14}$$

The standard thermodynamic parameters of R1233zd(E) are obtained through the NIST standard reference database of thermodynamic and transport properties of refrigerants.

In order to more intuitively describe the relative velocity magnitude of the gas phase and the liquid phase, the superficial velocities of the gas phase and the liquid phase are introduced and defined as:

$$v_{v,su} = \frac{G \bullet x}{\rho_v} \tag{15}$$

$$v_{l,su} = \frac{G \bullet (1-x)}{\rho_l} \tag{16}$$

3. Results and discussions

In this study, multiple groups of visual experiment cases are designed, which are shown in Table 3 together with their inlet detail parameters. Then, the influence of the inlet method (Case_1, Case_2 and Case_3), inlet quality (Case_4, Case_5 and Case_6) and inlet mass flux (Case_3, Case_4 and Case_7) can be fully contrasted for in-depth analysis. The temperature of inlet refrigerant R1233zd(E) is maintained at approximately 30 °C, and the two-phase physical parameters of the refrigerant are shown in Table 4.

3.1. The influence of inlet method

The phase distribution images and quantitative distribution curves (including mass flow ratio $FR_{m,i}$ and average void fraction α_i) under

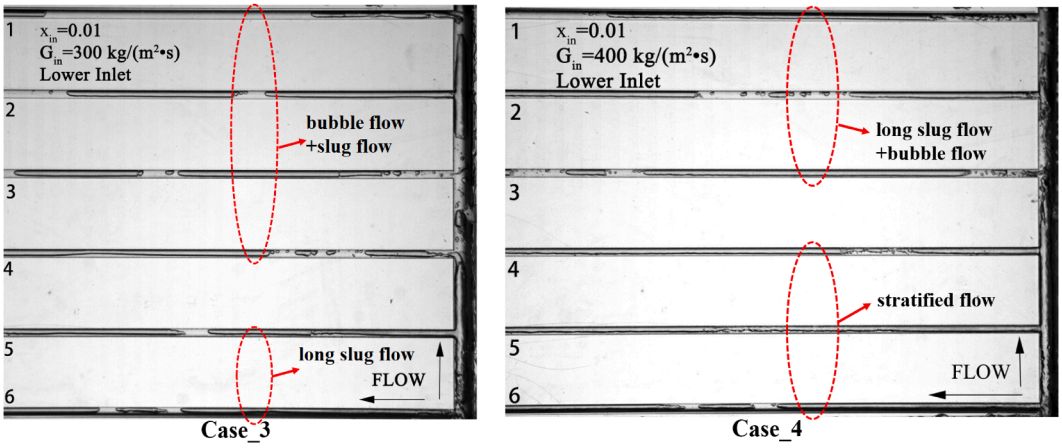

(a) G_{in}=300 kg/(m^2•s) (b) G_{in}=400 kg/(m^2•s)

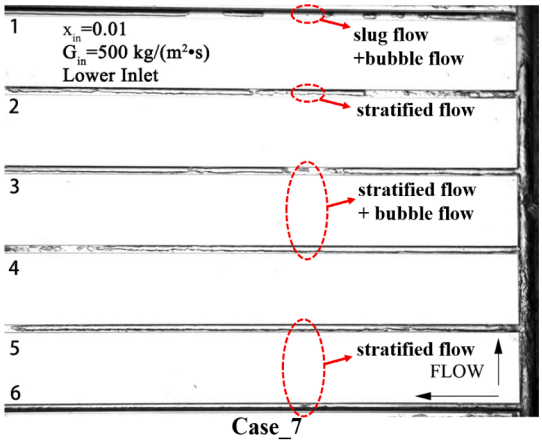

(c) G_{in}=500 kg/(m^2•s)

Fig. 9. Typical phase distribution images under different inlet mass flux.

different inlet methods are presented in Fig. 5. It should be emphasized that for each case there are thousands of images and they are all different. Therefore, to produce the curves, statistical averages are used, and for the visualization images a typical one is selected and displayed.

For the upper inlet method (Case_1), it can be seen that most of the liquid phase is transported to the bottom two channels (channel 5 and channel 6). This is because when the two-phase refrigerant enters from the upper position, the direction of the inertial force and the gravity is straight down. Under the superposition of the two main forces, the liquid phase is significantly affected and accumulates in the channel below. Additionally, the gas phase is blocked by the liquid column below, so the gas phase is mainly concentrated in the upper four channels. The flow patterns in the upper four channels are mainly stratified flow and annular flow, but the lower two channels are bubble flow and single-phase flow. From top to bottom, the flow patterns in the channels have undergone major changes. The local enlarged images of the partial flow channels are also shown in Fig. 5, which can more clearly observe the flow patterns and distinguish the differences between the flow patterns.

For the middle inlet method (Case_2), the quantitative distribution curves shown in Fig. 6(b) are similar to those in Case_1, as shown in Fig. 6(a). But the typical visualization image (Fig. 5(b)) is also different to Case_1 (Fig. 5(a)). That is because when the middle inlet method is adopted, the inlet configuration is similar to an impact T-junction [39]. Under this circumstance the inlet liquid phase momentum is mainly dissipated, and the liquid phase is transported to the two channels below due to gravity. Also, the gas phase is blocked by the liquid column so it is primarily transported to the upper four channels. The flow patterns in the upper four channels are mainly slug flow and stratified flow, and the lower two channels are mainly bubble flow.

Finally, for the lower inlet method (Case_3), it can be seen from Fig. 5 (c) and Fig. 6(c) that the visualization image and the quantitative distribution curves are very different to previous cases (Case_1 and Case_2). This is because when the two-phase refrigerant flow enters from the bottom, the gravity and the inertial force are in different directions. The gravity can offset the influence of inertial force to a great extent, so the flow distribution in each channel tends to be uniform. But the inertial force upward still dominates under this condition, so more refrigerant passes through the upper three channels (Fig. 6(c)). And because it is easier for the gas phase to enter the side branch [40], the average void fraction α_i tends to increase from the top to the bottom. The flow patterns in all channels are mainly slug flow, which demonstrates relative consistency.

The RSD of the mass and phase distribution under different inlet methods is shown in Fig. 6(d), and a smaller RSD value indicates improved uniformity. Compared with the middle inlet method, the value of RSD under the lower inlet method is reduced by 50–90%; compared with the upper inlet method, the value of RSD under the lower inlet method is reduced by 80–90%. It is clear that adopting the lower inlet method results in the best mass and phase distribution uniformity. The middle inlet method is next and the upper inlet method achieves the worst mass distribution uniformity. Therefore, the inlet method has a

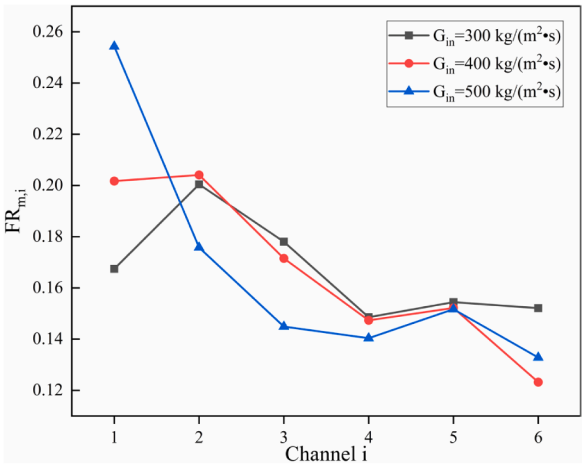

(a) the mass flow ratio distribution curves

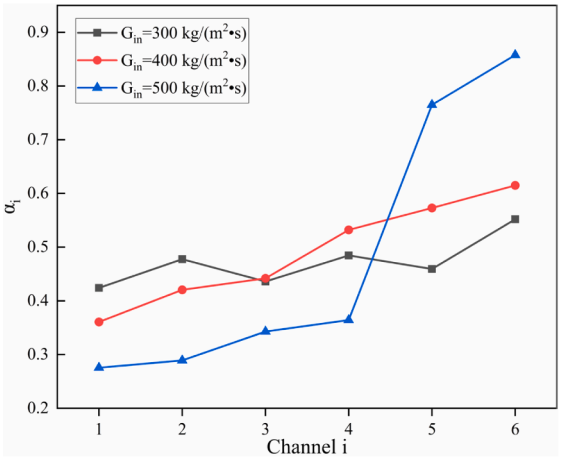

(b) the void fraction distribution curves

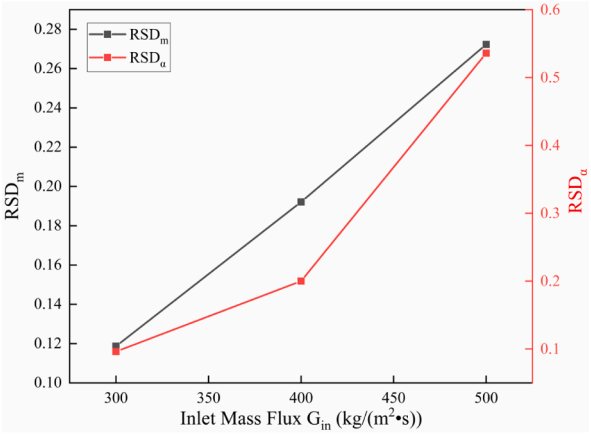

(c) the RSD curves of both

Fig. 10. The quantitative distribution and RSD curves under different inlet mass flux.

significant influence on the flow and phase distribution in branches.

3.2. *The influence of inlet quality*

The typical phase distribution images under different inlet quality data are shown in Fig. 7. It is clear that the flow pattern in the channel gradually changes from bubble flow and slug flow to churn flow and annular flow. When the inlet quality is at a relatively low level (Case_4 and Case_5), stratified flow will appear in the channels near the bottom, due to gravity and the gradually increasing velocity of the two-phase flow. But when the inlet quality is relatively high (Case_6), compared with gravity, the stronger gas-liquid two-phase inertial force makes it easier to form churn flow or annular flow in the channels.

The quantitative distribution and RSD curves of the mass flow ratio and the void fraction under different inlet quality data are displayed in Fig. 8. It is apparent from Fig. 8(a) that with the increase of inlet quality, the mass flow ratio in channel 1 $FR_{m,1}$ increases significantly. This is because when inlet quality increases, the inlet liquid superficial velocity decreases slightly while the inlet gas superficial velocity multiples as shown in Table 3, which means that the inlet gas phase inertial force cannot be ignored. The gas liquid two-phase interphase force also increases, which results in more liquid refrigerant flowing into the top channel (channel 1). The distribution uniformity in the channels deteriorates. Fig. 8(b) shows the average void fraction distribution curves in the channels, and it is apparent that it is easier for the gas phase to penetrate the channels closer to the inlet, so there is more gas in the channels near the bottom. In addition, with the increase of inlet quality, the void fraction in all the channels will increase, but the increase rate is decreasing. Finally, compared with the medium inlet quality, the value of RSD under the low inlet quality is reduced by 20–50%; compared with the high inlet quality, the value of RSD under the low inlet quality is reduced by 10–60%. The RSD curves in Fig. 8(c) indicate that there will be a more uniform two-phase distribution in the cold plate when the inlet quality is rather low within the scope of experimental conditions.

3.3. *The influence of inlet mass flux*

Similarly, the typical phase distribution images under different inlet mass flux are shown in Fig. 9. Different from the working conditions when the inlet quality varies, the flow pattern in the channel gradually changes from bubble flow and slug flow to stratified flow. It can be seen in Table 3 that when the inlet mass flux increases, the liquid phase superficial velocity and the gas phase superficial velocity increase in the same proportion and they do not increase significantly, which indicates that gravity still has a relatively important impact in these conditions. So stratified flow appears in most of the channels when the inlet mass flux increases to 500 kg/(m²•s) (Case_7).

The quantitative distribution and RSD curves of the mass flow ratio and the void fraction under different inlet mass flux are shown in Fig. 10. From Fig. 10(a) it can be clearly observed that when the inlet mass flux

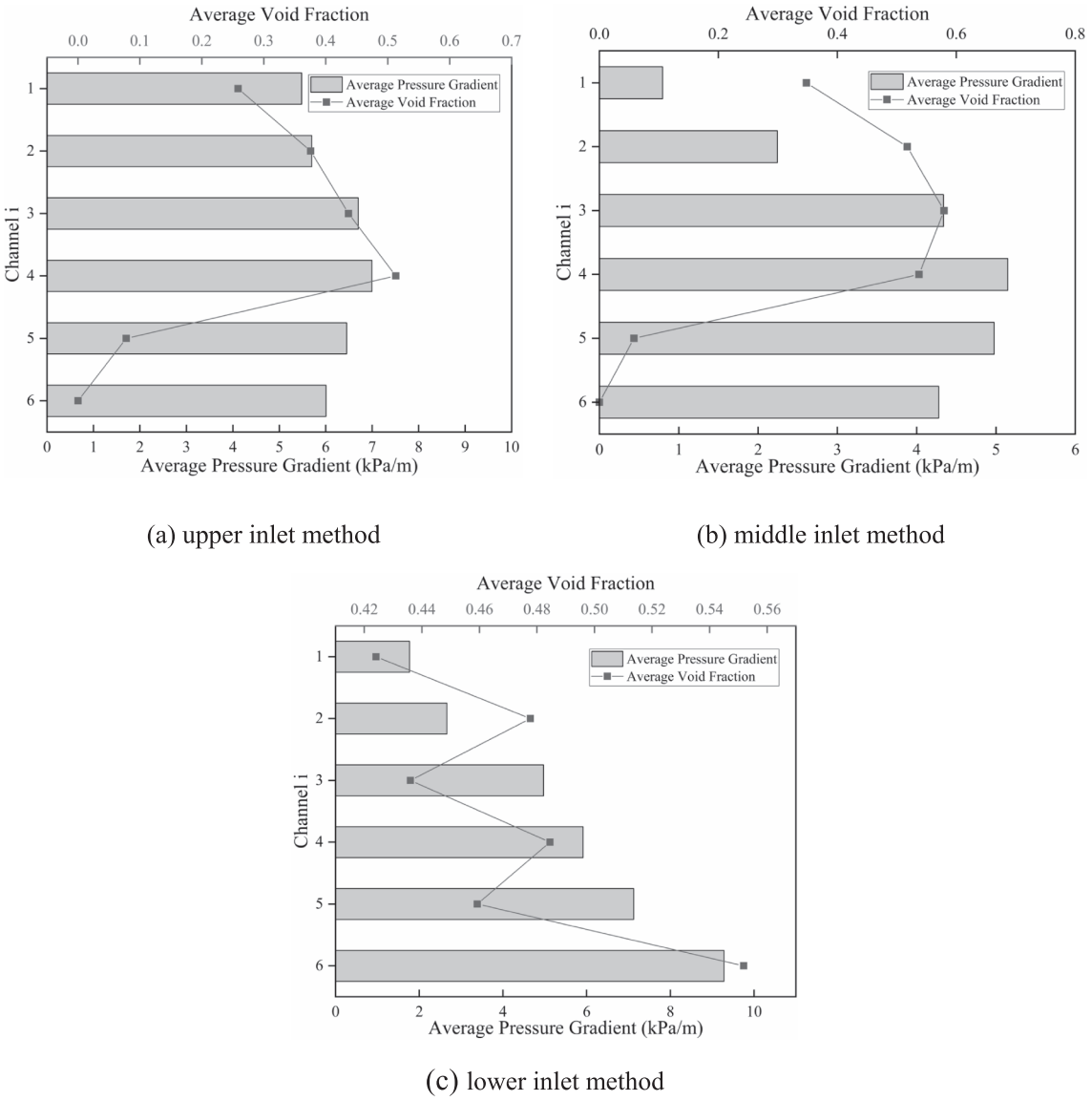

Fig. 11. The quantitative distribution of channel pressure gradient under different inlet methods.

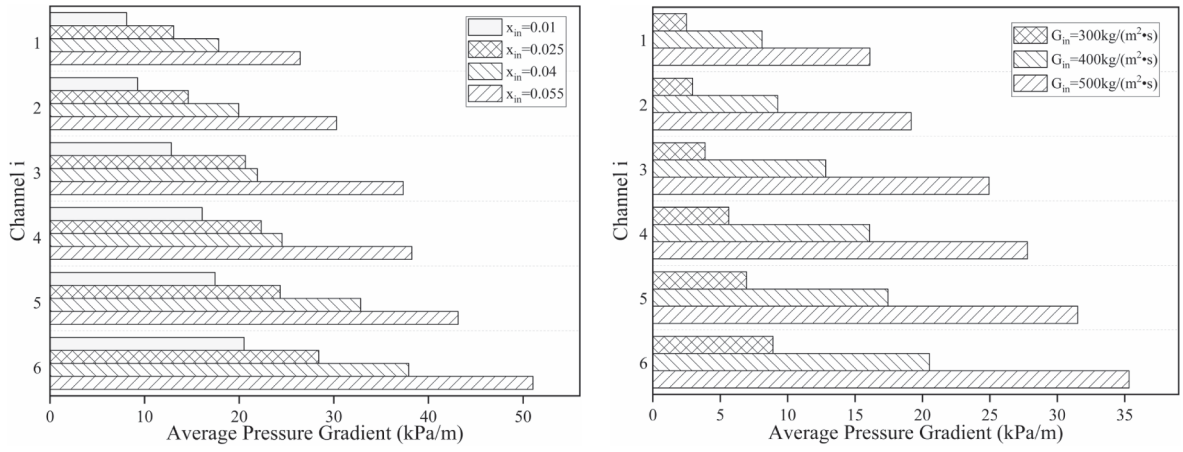

Fig. 12. Average pressure gradient in channels by different inlet quality and inlet mass flux.

increases, the mass flow ratio in channel 1 $FR_{m,1}$ also increases significantly, similar to Fig. 8(a), but the internal mechanisms are different. The gas phase superficial velocity has very limited growth (shown in Table 3), so the interphase force can be ignored in Fig. 10(a). It is the increased liquid phase momentum that causes the liquid phase to be more easily transported to the top channel (channel 1), which will also deteriorate the uniformity of the two-phase distribution. The average void fraction distribution curves in channels are shown in Fig. 10(b), and it is apparent that when the inlet mass flux increases, it is easier for the gas phase to penetrate the channels near the inlet. This is because the momentum of the gas phase is relatively small compared with the liquid phase, so the gas phase movement direction changes more easily. Also, compared with the medium inlet mass flux, the value of RSD under the low inlet mass flux is reduced by 40–50%; compared with the high inlet mass flux, the value of RSD under the low inlet mass flux is reduced by 60–80%. It can be seen from Fig. 10(c) that a lower inlet mass flux will achieve an improved two-phase distribution in the cold plate heat exchanger, but this conclusion is contrary to the study of Redo et al. [27]. However, the inlet mass flux range in their work was 50–250 kg/(m^2•s), so it is acceptable to deduce that the inlet mass flux has an appropriate value range for a specific condition in which an improved gas liquid two-phase uniformity can be achieved.

3.4. The relationship between pressure gradient and void fraction in channels

In order to further explore the mechanism of the distribution of the void fraction in channels, the average pressure gradient in channels, which can represent the resistance in channels, is calculated and compared with the average void fraction in this section. Fig. 11 shows the quantitative distribution of channel pressure gradient under different inlet methods. It is apparent from Fig. 11(a)(b)(c) and Fig. 5(a)(b)(c) that under most flow patterns (except bubble flow and single phase flow), the average pressure gradient and the average void fraction are positively correlated.

Fig. 12 shows the average pressure gradient in channels by different inlet quality and inlet mass flux, respectively. It can be seen from Fig. 12(b) and Fig. 10(b) that the average pressure gradient in channels is also positively correlated with the average void fraction. However, from Fig. 12(a) and Fig. 8(b), it seems that the correlation between the average pressure gradient and the average void fraction is weakened. The reason is that the inlet gas phase momentum flux multiples many times when the inlet quality increases. This is different from all the other cases. In that scenario (shown in Fig. 8(b)), the momentum of the gas phase cannot be ignored and the gas phase can be more easily transported to the channels slightly further away from the inlet. Therefore, it can be concluded that when the velocity difference between the gas phase and the liquid phase is small, the average pressure gradient and the average void fraction are almost always positively correlated, but the correlation is weakened when the velocity difference is large.

4. Conclusions

In order to explore the flow pattern and phase distribution characteristics of the two-phase refrigerant in each channel, a visual two-phase refrigerant flow distribution test bench, based on a cold plate type heat exchanger with six parallel small channels is built in this study. Three operating variables (inlet method, inlet quality and inlet mass flux) are analyzed on the uniformity of the two-phase distribution using the mass flow ratio and the void fraction obtained by image processing based on OpenCV. Furthermore, the relationship between pressure gradient and void fraction in channels is revealed. The following conclusions are drawn:

(1) Adopting the lower inlet method will achieve the best two-phase distribution uniformity because of the balance of the gravity on the inertial force, while the middle inlet method is next and finally, the upper inlet method achieves the poorest level of uniformity. Meanwhile, the maldistribution is more obvious when the inlet quality and inlet mass flux is relatively high (xin = 0.07, Gin = 500 kg/(m^2•s)). In addition, when the velocity difference between the gas phase and the liquid phase is small, the average pressure gradient and the average void fraction are usually positively correlated, but the correlation is weakened when the velocity difference is significant.

(2) The heat source was not applied to the heat exchanger in this study and future work could consider the influence of the heat load on the uniformity of two-phase distribution in channels, in order to meet the heat transfer requirements of actual battery modules. It is also necessary to further explore the influence of different working fluids on the phase separation uniformity, which will help to select refrigerants suitable for the heat pump thermal management system.

Declaration of Competing Interest

The authors declare that they have no known competing financial interests or personal relationships that could have appeared to influence the work reported in this paper.

Acknowledgements

The authors would like to thank the National Natural Science Foundation of China (Grant number 52076193) for their financial support.

References

[1] J. Kim, J. Oh, H. Lee, Review on battery thermal management system for electric vehicles, Appl. Therm. Eng. 149 (2019) 192–212.
[2] J. Li, W. Zuo, J. E, Y. Zhang, Q. Li, K. Sun, K. Zhou, G. Zhang, Multi-objective optimization of mini U-channel cold plate with SiO_2 nanofluid by RSM and NSGA-II, Energy 242 (2022) 123039.
[3] Y. Huang, S. Wang, Y. Lu, R. Huang, X. Yu, Study on a liquid cooled battery thermal management system pertaining to the transient regime, Appl. Therm. Eng. 180 (2020), 115793.
[4] K. Monika, C. Chakraborty, S. Roy, S. Dinda, S.A. Singh, S.P. Datta, Parametric investigation to optimize the thermal management of pouch type lithium-ion batteries with mini-channel cold plates, Int. J. Heat Mass Transf. 164 (2021), 120568.
[5] W.X. Wu, S.F. Wang, W. Wu, K. Chen, S.H. Hong, Y.X. Lai, A critical review of battery thermal performance and liquid based battery thermal management, Energy Convers. Manage. 182 (2019) 262–281.
[6] S.H. Hong, D.S. Jang, S. Park, S. Yun, Y. Kim, Thermal performance of direct two-phase refrigerant cooling for lithium-ion batteries in electric vehicles, Appl. Therm. Eng. 173 (2020), 115213.
[7] T. Xiong, G. Liu, S. Huang, G. Yan, J. Yu, Two-phase flow distribution in parallel flow mini/micro-channel heat exchangers for refrigeration and heat pump systems: A comprehensive review, Appl. Therm. Eng. 201 (2022) 117820, https://doi.org/10.1016/j.applthermaleng.2021.117820.
[8] M. Shen, Q. Gao, Structure design and effect analysis on refrigerant cooling enhancement of battery thermal management system for electric vehicles, J. Storage Mater. 32 (2020), 101940.
[9] A.T. Wijayanta, T. Miyazaki, S. Koyama, Note on refrigerant R134a flow maldistribution in a header type evaporator, Int. J. Refrig 95 (2018) 1–9.
[10] N.H. Kim, C.H. Kim, Y. Shah, W. Li, Improvement of two-phase refrigerant distribution for upward flow of a parallel flow minichannel heat exchanger using insertion devices, Appl. Therm. Eng. 160 (2019), 114065.
[11] A.J. Mahvi, S. Garimella, Modeling framework to predict two-phase flow distribution in heat exchanger headers, Int. J. Refrig 104 (2019) 65–75.
[12] W.-J. Lee, J.H. Jeong, Development of a numerical analysis model for a multi-port mini-channel heat exchanger considering a two-phase flow distribution in the header. Part I: Numerical modeling, Int. J. Heat Mass Transfer 138 (2019) 1264–1280.
[13] Y. Zou, H. Tuo, P.S. Hrnjak, Modeling refrigerant maldistribution in microchannel heat exchangers with vertical headers based on experimentally developed distribution results, Appl. Therm. Eng. 64 (2014) 172–181.
[14] N.H. Kim, H.W. Byun, Effect of inlet configuration on upward branching of two-phase refrigerant in a parallel flow heat exchanger, Int. J. Refrig. 36 (2013) 1062–1077.

[15] U. Madanan, D. Chatterjee, S.K. Das, A note on adiabatic two-phase flow maldistribution in a set of horizontal parallel minichannels with I-type and Z-type configurations, Chem. Eng. Process.-Process Intensificat. 132 (2018) 34–41.
[16] N.H. Kim, M.G. Go, Horizontal distribution of two-phase refrigerant in parallel flat mini-channels, Exp. Therm Fluid Sci. 93 (2018) 139–152.
[17] A. Marchitto, M. Fossa, G. Guglielmini, The effect of the flow direction inside the header on two-phase flow distribution in parallel vertical channels, Appl. Therm. Eng. 36 (2012) 245–251.
[18] X. Wu, Z. Gao, H. Meng, Y. Wang, C. Cheng, Experimental study on the uniform distribution of gas-liquid two-phase flow in a variable-aperture deflector in a parallel flow heat exchanger, Int. J. Heat Mass Transf. 150 (2020), 119353.
[19] Y. Zhang, W. Zuo, J. E, J. Li, Q. Li, K. Sun, K. Zhou, G. Zhang, Performance comparison between straight channel cold plate and inclined channel cold plate for thermal management of a prismatic $LiFePO_4$ battery, Energy 248 (2022) 123637.
[20] Y. Liu, S. Wang, Distribution of gas-liquid two-phase slug flow in parallel micro-channels with different branch spacing, Int. J. Heat Mass Transf. 132 (2019) 606–617.
[21] A. Marchitto, M. Fossa, G. Guglielmini, Phase split in parallel vertical channels in presence of a variable depth protrusion header, Exp. Therm Fluid Sci. 74 (2016) 257–264.
[22] Y. Li, X. Luo, Z. Wang, Z. Yang, J. Chen, Y. Liang, C. Wang, Y. Chen, Numerical simulation on the header-orifice structure-based liquid-vapor separator used in liquid-separation condenser, Chem. Eng. Sci. 235 (2021), 116475.
[23] W. Zuo, J. Li, Y. Zhang, Q. Li, S. Jia, Z. He, Multi-factor impact mechanism on combustion efficiency of a hydrogen-fueled micro-cylindrical combustor, Int. J. Hydrogen Energy 45 (2020) 2319–2330.
[24] W. Zuo, J. Li, Y. Zhang, Q. Li, Z. He, Effects of multi-factors on comprehensive performance of a hydrogen-fueled micro-cylindrical combustor by combining grey relational analysis and analysis of variance, Energy 199 (2020), 117439.
[25] Y. Zou, P.S. Hrnjak, Experiment and visualization on R134a upward flow in the vertical header of microchannel heat exchanger and its effect on distribution, Int. J. Heat Mass Transf. 62 (2013) 124–134.
[26] Y. Zou, P.S. Hrnjak, Refrigerant distribution in the vertical header of the microchannel heat exchanger-Measurement and visualization of R410A flow, Int. J. Refrig. 36 (2013) 2196–2208.
[27] M.A. Redo, J. Jeong, N. Giannetti, K. Enoki, S. Yamaguchi, K. Saito, H. Kim, Characterization of two-phase flow distribution in microchannel heat exchanger header for air-conditioning system, Exp. Therm Fluid Sci. 106 (2019) 183–193.
[28] N.H. Kim, D.Y. Kim, H.W. Byun, Effect of inlet configuration on the refrigerant distribution in a parallel flow minichannel heat exchanger, Int. J. Refrig. 34 (2011) 1209–1221.
[29] M.A. Redo, J. Jeong, S. Yamaguchi, K. Saito, H. Kim, Characterization and improvement of flow distribution in a vertical dual-compartment header of a microchannel heat exchanger, Int. J. Refrig. 116 (2020) 36–48.
[30] A.T. Wijayanta, T. Miyazaki, S. Koyama, Refrigerant distribution in horizontal headers with downward minichannel-branching conduits: Experiment, empirical correlation and two-phase flow pattern map, Exp. Therm Fluid Sci. 81 (2017) 430–444.
[31] M. Masiukiewicz, S. Anweiler, Two-phase flow structure assessment based on dynamic image analysis, Flow Meas. Instrum. 65 (2019) 195–202.
[32] G. Rafałko, R. Mosdorf, G. Górski, Two-phase flow pattern identification in minichannels using image correlation analysis, Int. Commun. Heat Mass Transfer 113 (2020), 104508.
[33] S. Park, D.S. Jang, D. Lee, S.H. Hong, Y. Kim, Simulation on cooling performance characteristics of a refrigerant-cooled active thermal management system for lithium ion batteries, Int. J. Heat Mass Transf. 135 (2019) 131–141.
[34] S. Saisorn, P. Wongpromma, S. Wongwises, The difference in flow pattern, heat transfer and pressure drop characteristics of mini-channel flow boiling in horizontal and vertical orientations, Int. J. Multiph. Flow 101 (2018) 97–112.
[35] Y. Liu, W. Sun, W. Wu, S. Wang, Gas-liquid two-phase flow distribution in parallel micro-channels with different header and channels' orientations, Int. J. Heat Mass Transf. 112 (2017) 767–778.
[36] A. Marchitto, M. Fossa, Enhancing the phase distribution in parallel vertical channels with single and double chamber coaxial headers, Appl. Therm. Eng. 155 (2019) 239–246.
[37] F. Polonara, L. Kuijpers, R. Peixoto, Potential impacts of the montreal protocol kigali amendment to the choice of refrigerant alternatives, Int. J. Heat Technol. 35 (Special Issue1) (2017) S1–S8.
[38] N. Ghendour, M. Meribout, A. Azzi, Review of measurement techniques for void fraction of two-phase flow through annulus, Measurement 165 (2020), 108196.
[39] N. Zheng, L. Zhao, Y. Hwang, J. Zhang, X. Yang, Experimental study on two-phase separation performance of impacting T-junction, Int. J. Multiph. Flow 83 (2016) 172–182.
[40] J. Chen, S. Wang, S. Cheng, Experimental investigation of two-phase distribution in parallel micro-T channels under adiabatic condition, Chem. Eng. Sci. 84 (2012) 706–717.